Exhaust emissions estimation during transient turbocharged diesel engine operation using a two-zone combustion model

C.D. Rakopoulos, A.M. Dimaratos, E.G. Giakoumis* and D.C. Rakopoulos

Internal Combustion Engines Laboratory,
Thermal Engineering Department,
School of Mechanical Engineering,
National Technical University of Athens,
9 Heroon Polytechniou Street,
Zografou Campus 15780, Athens, Greece
E-mail: cdrakops@central.ntua.gr
E-mail: adim@central.ntua.gr
E-mail: vgiakms@central.ntua.gr
E-mail: dimracop@central.ntua.gr
*Corresponding author

Abstract: A comprehensive, two-zone, transient, diesel combustion model is used to study the performance and exhaust emissions of a turbocharged diesel engine during load transients. Analytical modelling of fuel spray and in-cylinder processes is included, while detailed equations concerning all engine sub-systems describe the phenomena, which diversify transient operation from the steady-state. Demonstrative diagrams are provided for the time histories of nitric oxide (NO) and soot emissions during transient operation, and the main factors affecting their formation are highlighted. Moreover, in-cylinder development of NO concentration and soot density during individual transient cycles is provided and compared with their respective steady-state counterparts. This comparison points out the differences between steady-state and transient operation, as regards exhaust emissions development. The study is expanded with the investigation of load change magnitude and cylinder wall insulation effects on transient emissions.

Keywords: exhaust emissions; insulation; nitric oxide; NO concentration; soot density; transient operation; turbocharged diesel engine; two-zone model.

Reference to this paper should be made as follows: Rakopoulos, C.D., Dimaratos, A.M., Giakoumis, E.G. and Rakopoulos, D.C. (2009) 'Exhaust emissions estimation during transient turbocharged diesel engine operation using a two-zone combustion model', *Int. J. Vehicle Design*, Vol. 49, Nos. 1/2/3, pp.125–149.

Biographical notes: Constantine D. Rakopoulos is the Dean of the School of Mechanical Engineering, Full Professor of Internal Combustion Engines and Director of the I.C. Engines Laboratory at the School of Mechanical Engineering of the National Technical University of Athens (NTUA), Greece. He graduated from the NTUA and obtained his MSc, DIC and PhD from Imperial College of Science, Technology and Medicine, University of London, UK. He has been responsible for the development of engines research at the School of Mechanical Engineering of the NTUA for the last 30 years, with over 170 refereed papers in international journals and conferences.

Athanasios M. Dimaratos is Dipl. Ing. from the School of Mechanical Engineering of the National Technical University of Athens, Greece. He is a Research Assistant at the Internal Combustion Engines Laboratory of the NTUA and he is currently working on his PhD thesis.

Evangelos G. Giakoumis is Dipl. Ing. and Dr. Ing. from the School of Mechanical Engineering of the National Technical University of Athens, Greece. He has worked for 6 years as Area Manager at the After Sales Department of the Peugeot Automobiles Distributor in Greece, and is now a Lecturer at the Thermal Engineering Department of the School of Mechanical Engineering of the NTUA. His research interests include diesel engine experimental and simulation analysis under transient conditions, second law analysis of internal combustion engines and use of alternative fuels.

Dimitrios C. Rakopoulos is Dipl. Ing. and Dr. Ing. from the School of Mechanical Engineering of the National Technical University of Athens, Greece. He is a Research Associate at the Internal Combustion Engines Laboratory of the NTUA. His research interests include diesel engine modelling and experimental investigation, exhaust emissions and alternative-biological fuels.

Nomenclature

A	surface area (m^2)
D	cylinder bore (m)
D_N	injector nozzle hole diameter (m)
E	internal energy (J) or activation energy (J $kmol^{-1}$)
E_{red}	reduced activation energy (K)
F	force (N)
G	moment of inertia (kg m^2)
h	specific enthalpy (J kg^{-1})
k_f	forward reaction rate constant (m^3 $kmol^{-1}$ sec^{-1})
L_N	injector nozzle hole length (m)
L_{rod}	connecting rod length (m)
m	mass (kg)
M	molecular weight (kg $kmol^{-1}$)
N	engine rotational speed (rpm)
p	pressure (N m^{-2})
P	combustion model preparation rate (kg CA^{-1})
Q	heat (J)

r	crank radius (m)
R	combustion model reaction rate (kg CA^{-1})
R_{mol}	universal gas constant (8314.3 J $kmol^{-1}$ K^{-1})
S	piston stroke (m)
t	time (sec)
T	temperature (K)
$\bar{u}_{pist}$	mean piston velocity (m sec^{-1})
V	volume (m^3)
X	fuel spray tip penetration (m)

Greek symbols

θ	fuel spray angle (degree)
ρ	density (kg m^{-3})
τ	torque (Nm)
φ	crank angle (degree)
Φ	fuel-air equivalence ratio
ω	angular speed (rad sec^{-1})

Subscripts

a	air
br	fuel jet break-up point
ch	charge
e	engine
f	fuel
fr	friction
g	gas
inj	injected
L	loss or load
s	swirl
sc	soot oxidised
sf	soot formed
sn	soot net
up	unprepared
w	wall

Abbreviations

°CA	degree crank angle
BMEP	brake mean effective pressure (bar)
EGR	exhaust gas recirculation
EVO	exhaust valve opening
FMEP	friction mean effective pressure (bar)
IVC	inlet valve closure
NO	nitric oxide
PSZ	plasma spray zirconia
rpm	revolutions per minute
SN	silicon nitride
TDC	top dead centre

1 Introduction

Nowadays, the turbocharged diesel engine is the most preferred prime mover in medium and medium-large units applications (truck driving, land traction, ship propulsion and electrical generation). Moreover, it continuously increases its share in the highly competitive automotive market owing to its reliability that is combined with excellent fuel efficiency. Particularly, its transient operation is of great importance in everyday operating conditions of engines, being often linked with off-design and consequently non-optimum performance. Turbocharger lag is the most notable off-design feature of diesel engine transient operation that significantly differentiates the torque pattern from the respective steady-state conditions. It is caused because, although the fuel pump responds rapidly to the increased fuelling demand after a load or speed increase, the turbocharger compressor air-supply cannot match this higher fuel-flow instantly, but only after a number of engine cycles owing to the inertia of the whole system; the above phenomenon is enhanced by the unfavourable turbocharger compressor characteristics at low loads and speeds. As a result of this slow reaction, the relative air–fuel ratio during the early cycles of a transient event assumes very low values (even lower than stoichiometric) deteriorating combustion and leading to slow engine (torque and speed) response, long recovery period and overshoot in particulate, gaseous and noise emissions. On the other hand, the high fuel-air equivalence ratios experienced after a speed or load increase transient event, produce high combustion temperatures favouring nitric oxide (NO) and soot formation, with the latter being identified as black smoke coming out of the exhaust pipe (Rakopoulos and Giakoumis, 2006a).

During the last decades, diesel engine modelling has intensively supported the study of engine operation under transient conditions with simulations of various levels of complexity. Extensive studies have been conducted for a variety of purposes, such

as investigation of the effect of various parameters on engine transient response (Watson and Janota, 1982; Winterbone, 1986; Benajes, Luján and Serrano, 2000; Rakopoulos et al., 2004a; Rakopoulos and Giakoumis, 2006b), ways of improving response (Watson, 1984; Rakopoulos and Giakoumis, 2006a), compressor surging (Rakopoulos, Michos and Giakoumis, 2005), second-law balance (Rakopoulos and Giakoumis, 2004) and issues concerning engine dynamics (Rakopoulos, Giakoumis and Dimaratos, 2007).

The study of exhaust emissions during transients – although of primary concern to engine manufacturers since newly produced engines must meet the stringent emission regulations following a legislated transient cycle – has been dealt with so far mainly on an experimental basis (Kang and Farell, 2005; Hagena, Filipi and Assanis, 2006). On the other hand, the majority of transient models have not included exhaust emissions prediction in their simulations. The latter emanates from a compromise that has to be made, since transient simulations require relatively high computational time, which would become prohibitive if exhaust emissions prediction were also included. Thus, transient codes incorporating a multi-or even a two-zone combustion model are scarce (Bazari, 1994; Chan, He and Sun, 1999), with the latter reference addressing NO emissions predictions only. On the other hand, approximations using quasi-linear models that are based on steady-state engine performance fail to predict accurately exhaust emissions during transients, especially so for the turbocharger lag cycles (Hagena, Filipi and Assanis, 2006), since no actual modelling of the relevant off-design phenomena is included.

The aim of the present work is to fill this apparent gap in the open literature by conducting a preliminary assessment of NO and soot exhaust emissions during transient operation of a turbocharged diesel engine. To achieve this target, an experimentally validated two-zone transient diesel combustion model is used, having the added advantage of limited requirements in terms of execution time and computer memory. Analytical modelling of in-cylinder processes, such as air motion, fuel spray development, wall impingement and combustion chemistry is included, and detailed equations concerning all engine sub-systems describe the phenomena, which diversify transient from steady-state operation. The results of the study will be given in a series of diagrams, which depict exhaust emissions development during transient operation. The response of important engine parameters, such as fuel-air equivalence ratio or charge temperature, will be also provided. In addition, individual intermediate transient cycles will be studied in comparison to their steady-state counterparts, in terms of in-cylinder NO and soot formation. Owing to the narrow speed range of the engine in hand, mainly load increases with constant governor setting are investigated, which, nonetheless, play a significant role in the European or American transient cycles of heavy duty engines.

2 In-cylinder processes modelling

2.1 Two-zone model description – conservation and state equations

The model incorporates all the processes taking place in the cylinder, i.e. in-cylinder air motion, fuel spray development and mixing, spray impingement on the walls, turbulent heat transfer and combustion chemistry. Droplets evaporation and fuel ignition delay are implicitly taken into account through the combustion sub-model. The fuel is assumed to be dodecane ($C_{12}H_{26}$) with a lower heating value LHV = 42,500 kJ kg^{-1}. The evaluation

of the thermodynamic processes is based on the first law of thermodynamics and the perfect gas state equation.

Regarding fuel spray development and air entrainment processes, these have been analysed in detail previously (Rakopoulos, Rakopoulos and Kyritsis, 2003). For article completeness, however, a brief description is given in Appendix A.

Two separate zones in the cylinder are identified, namely the air (unburned) zone consisting of pure air, and the fuel spray (burned) zone consisting of the combustion products, injected fuel and the incoming air from the air-zone. During compression, only one zone exists (that of pure air). Thus, the first law of thermodynamics for a closed system and the perfect gas state equation read (Heywood, 1988)

$$\mathrm{d}Q = \mathrm{d}E + p\mathrm{d}V \tag{1}$$

$$pV = m\frac{R_{\mathrm{mol}}}{M_{\mathrm{ch}}}T \tag{2}$$

where $\mathrm{d}Q$ is the heat loss to the cylinder walls, M_{ch} the charge molecular weight and V the instantaneous cylinder volume given as function of crank angle φ by

$$V(\varphi) = V_{\mathrm{cl}} + \frac{\pi D^2}{4}\left[r(1-\cos\varphi) + L_{\mathrm{rod}}\left(1-\sqrt{1-\lambda^2\sin^2\varphi}\right)\right] \tag{3}$$

where V_{cl} is the cylinder clearance volume and $\lambda = r/L_{\mathrm{rod}}$ the crank radius to connecting rod length ratio.

During combustion and expansion, both unburned and burned zones exist; the latter consists of all fuel sprays developed in the cylinder according to the number of injector nozzle holes. In this case, apart from the perfect gas state equation, the first law of thermodynamics for an open system is applied for each zone.

For the surrounding air-zone, which only loses air mass to the burning zone, the first law of thermodynamics is given by (Benson and Whitehouse, 1979)

$$\mathrm{d}Q = \mathrm{d}E + p\mathrm{d}V + h_{\mathrm{a}}\mathrm{d}m_{\mathrm{a}} \tag{4}$$

while for the burning zone, which gains air mass from the air-zone and also an enthalpic flow from the fuel prepared to be burned in the time step, the first law of thermodynamics is written in the form

$$\mathrm{d}Q = \mathrm{d}E + p\mathrm{d}V - h_{\mathrm{a}}\mathrm{d}m_{\mathrm{a}} - h_{\mathrm{f}}\mathrm{d}m_{\mathrm{f}} \tag{5}$$

Polynomial expressions according to the absolute temperature T are used concerning the calculation of internal energy and specific heat capacities for each species considered in the model (Benson and Whitehouse, 1979). The internal energy E in the above equations is then computed by knowing the instantaneous composition and the specific internal energy of each constituent.

After the calculation of the state in each zone, a mean state of the cylinder contents can be computed assuming isenthalpic mixing of the zones (Rakopoulos et al., 2004b).

2.2 Heat transfer model

The simulation of heat loss Q_L to the cylinder walls is based on the model proposed by Annand and Ma (1970–1971),

$$\frac{dQ_L}{dt} = A\left\{a\frac{k_g}{D}Re^b(T_g - T_w) + c\left(T_g^4 - T_w^4\right)\right\} \tag{6}$$

where a, b and c are constants evaluated after experimental matching at steady-state conditions. Further, $A = 2A_{pist} + A'$, with $A_{pist} = \pi D^2/4$ the piston cross section area and $A' = \pi Dx$ with x the instantaneous cylinder height in contact with the gas. Also, T_g is the absolute zone temperature and $Re = \rho \bar{u}_{pist} D/\mu_g$ is the Reynolds number; $\bar{u}_{pist} = 2NS/60$ is the mean piston speed with S the piston stroke, and k_g, μ_g are the gas thermal conductivity and viscosity, respectively, expressed as polynomial functions of temperature T_g. After the start of combustion, the total heat loss to the cylinder walls is distributed into the two-zones in proportion to their mass and absolute temperature (Shahed, Chiu and Lyn, 1975).

During transient operation, the thermal inertia of the cylinder wall is taken into account, using a detailed heat transfer scheme that models the temperature distribution from the gas to the cylinder walls up to the coolant.

2.3 Combustion model

The model proposed by Whitehouse and Way (1969–1970) is used for the calculation of the combustion rate. In this model, the combustion process consists of two parts; a preparation limited combustion rate and a reaction (Arrhenius type) limited combustion rate.

The preparation rate P (in kg CA^{-1}) is given by

$$P = Km_{f_{inj}}^{1-x} m_{f_{up}}^{x} p_{O_2}^{m} \tag{7}$$

while the reaction rate R (in kg CA^{-1}) is defined as

$$R = \frac{K' p_{O_2}}{N'\sqrt{T}} e^{-E_{red}/T} \int_0^{\varphi} (P - R)d\varphi \tag{8}$$

In the above relations, $m_{f_{inj}}$ is the cumulative fuel mass injected up to the current crank angle φ, which is expressed as

$$m_{f_{inj}} = \int_0^{\varphi} \frac{dm_{f_{inj}}}{d\varphi} d\varphi \tag{9}$$

where $dm_{f_{inj}}/d\varphi$ is the fuel injection rate. Moreover, $m_{f_{up}}$ is the cumulative fuel mass not yet prepared for combustion and is calculated by the relation

$$m_{f_{up}} = m_{f_{inj}} - \int_0^{\varphi} P \mathrm{d}\varphi \tag{10}$$

Also, N' is the engine speed in revolutions per second and p_{O_2} is the oxygen partial pressure (in bar) in the burning zone. Constants K, K', x, m and E_{red} are evaluated after experimental matching at steady-state conditions.

Finally, the combustion rate is defined by the following relations

$$\frac{\mathrm{d}m_{fb}}{\mathrm{d}\varphi} = \begin{cases} R, & \text{if} \quad R < P \\ P, & \text{if} \quad R > P \end{cases} \tag{11}$$

2.4 Calculation of combustion products

The complete chemical equilibrium scheme proposed by Way (1977) is used for the calculation of combustion products. The species considered are N_2, O_2, CO_2, H_2O, CO, H_2, NO, OH, N, H and O. The concentration of each one of the above species is calculated by solving a system of eleven equations, consisting of four atom balance equations (one for each element of the system C–H–O–N) and seven equilibrium equations. The chemical reactions considered in equilibrium, together with their respective equilibrium constants, are the following

$$\begin{aligned}
&(1)\ \ N_2 + O_2 \rightleftharpoons 2NO, && K_{p1} = p_{NO}^2 \Big/ \left(p_{N_2} \cdot p_{O_2} \right) \\
&(2)\ \ 2H_2O + O_2 \rightleftharpoons 4OH, && K_{p2} = p_{OH}^4 \Big/ \left(p_{H_2O}^2 \cdot p_{O_2} \right) \\
&(3)\ \ 2CO + O_2 \rightleftharpoons 2CO_2, && K_{p3} = p_{CO_2}^2 \Big/ \left(p_{CO}^2 \cdot p_{O_2} \right) \\
&(4)\ \ 2H_2 + O_2 \rightleftharpoons 2H_2O, && K_{p4} = p_{H_2O}^2 \Big/ \left(p_{H_2}^2 \cdot p_{O_2} \right) \\
&(5)\ \ N_2 \rightleftharpoons 2N, && K_{p5} = p_N^2 \Big/ p_{N_2} \\
&(6)\ \ H_2 \rightleftharpoons 2H, && K_{p6} = p_H^2 \Big/ p_{H_2} \\
&(7)\ \ O_2 \rightleftharpoons 2O, && K_{p7} = p_O^2 \Big/ p_{O_2}
\end{aligned} \tag{12}$$

where p_i are the partial pressures of the species, made dimensionless with respect to atmospheric pressure $p_{atm} = 1$ atm.

2.5 Nitric oxide formation model

Since, it is well established that NO formation is controlled by chemical kinetics rather than chemical equilibrium, the generally accepted kinetics model proposed by Lavoie, Heywood and Keck (1970) is adopted; it describes the extended Zeldovich kinetics scheme. According to this model, the governing chemical reactions for NO formation and their respective forward reaction rate constants are as follows

$$\begin{aligned} &\mathrm{N}+\mathrm{NO} \rightleftharpoons \mathrm{N}_2+\mathrm{O}, k_{1\mathrm{f}}=3.1\times10^{10}e^{(-160/T)} \\ &\mathrm{N}+\mathrm{O}_2 \rightleftharpoons \mathrm{NO}+\mathrm{O}, k_{2\mathrm{f}}=6.4\times10^{6}Te^{(-3125/T)} \\ &\mathrm{N}+\mathrm{OH} \rightleftharpoons \mathrm{NO}+\mathrm{H}, k_{3\mathrm{f}}=4.2\times10^{10} \end{aligned} \tag{13}$$

The one way equilibrium rates for the above three reactions are defined as

$$R_1=k_{1\mathrm{f}}(N)_e(\mathrm{NO})_e,\ R_2=k_{2\mathrm{f}}(N)_e(\mathrm{O}_2)_e,\ R_3=k_{3\mathrm{f}}(N)_e(\mathrm{OH})_e \tag{14}$$

where index '*e*' denotes equilibrium concentrations and term $\alpha=(\mathrm{NO})/(\mathrm{NO})_e$.

Finally, the rate of change of NO concentration is expressed as

$$\frac{1}{V}\frac{\mathrm{d}((\mathrm{NO})V)}{\mathrm{d}t}=2(1-\alpha^2)\frac{R_1}{1+\alpha\dfrac{R_1}{R_2+R_3}} \tag{15}$$

2.6 Net soot formation model

For the calculation of the net soot that is formed inside the cylinder, the model of Hiroyasu, Kadota and Arai (1983) is used, as modified by Lipkea and DeJoode (1994). The net soot formation rate is expressed as the difference of the formation and oxidation rates, which are given by

$$\frac{\mathrm{d}m_{\mathrm{sf}}}{\mathrm{d}t}=A_{\mathrm{sf}}\mathrm{d}m_{\mathrm{f}}^{0.8}p^{0.5}\ e^{\left(-E_{\mathrm{sf}}/(R_{\mathrm{mol}}T)\right)} \tag{16}$$

$$\frac{\mathrm{d}m_{\mathrm{sc}}}{\mathrm{d}t}=A_{\mathrm{sc}}m_{\mathrm{sn}}\left(p_{\mathrm{O}_2}/p\right)p^{n}\ e^{\left(-E_{\mathrm{sc}}/(R_{\mathrm{mol}}T)\right)} \tag{17}$$

where pressures are in bar and masses in kg, $\mathrm{d}m_{\mathrm{f}}$ is the fuel vapour mass to be burned in the current time step and p_{O_2} is the partial pressure of oxygen in the zone. Also, constants A_{sf}, A_{sc}, activation energies E_{sf}, E_{sc} and the exponent n are evaluated after experimental matching at steady-state conditions. Finally, the net soot formation rate is expressed as follows

$$\frac{\mathrm{d}m_{\mathrm{sn}}}{\mathrm{d}t}=\frac{\mathrm{d}m_{\mathrm{sf}}}{\mathrm{d}t}-\frac{\mathrm{d}m_{\mathrm{sc}}}{\mathrm{d}t}. \tag{18}$$

3 Dynamic analysis

3.1 Friction modelling

For the computation of friction inside the cylinder, the model proposed by Taraza, Henein and Bryzik (2000) is adopted. It describes the non-steady profile of friction torque during each engine cycle, based on fundamental friction analysis. According to this approach, the total amount of friction at each degree crank angle (°CA) is the summation

of four terms, i.e. piston rings assembly (including piston rings and piston skirt contribution), loaded bearings, valve train and auxiliaries. The important feature of the specific model is that it accounts for the considerable variation of friction torque during the engine cycle (especially around 'hot' top dead centre (TDC)), unlike the usually applied 'mean' fmep equations where friction torque is assumed constant throughout each cycle.

3.2 Crankshaft torque equilibrium

The conservation of angular momentum applied to the total system (engine plus load), based on Newton's second-law of motion for rotational systems, is given by

$$\tau_{\mathrm{e}}(\varphi,\omega)-\tau_{\mathrm{fr}}(\varphi,\omega)-\tau_{\mathrm{L}}(\omega)=G_{\mathrm{tot}}\frac{\mathrm{d}\omega}{\mathrm{d}t} \tag{19}$$

where G_{tot} is the total mass moment of inertia of the system (engine-flywheel-brake). The term $\tau_{\mathrm{e}}(\varphi,\omega)$ represents the instantaneous engine indicated torque and includes gas, inertia and (the negligible) gravitational forces contribution; it is mostly dependent on accurate combustion modelling and is given explicitly by

$$\tau_{\mathrm{e}}(\varphi)=\overbrace{\tau_{\mathrm{g}}(\varphi)}^{\text{Gas}}+\overbrace{\tau_{\mathrm{in}}(\varphi)}^{\text{Inertia}}+\overbrace{\tau_{\mathrm{gr}}(\varphi)}^{\text{Gravitational}}=[p_{\mathrm{g}}(\varphi)\cdot A_{\mathrm{pist}}\cdot R_1(\varphi)+F_{\mathrm{Tin}}(\varphi)+F_{\mathrm{gr}}(\varphi)]\cdot r \tag{20}$$

where $p_{\mathrm{g}}(\varphi)$ is the instantaneous cylinder pressure and $R_1(\varphi)=u_{\mathrm{pist}}/r\omega$, with u_{pist} the instantaneous piston velocity. For the calculation of inertia force F_{Tin}, a detailed model is applied treating the connecting rod as a rigid body experiencing reciprocating and rotating movement at the same time (Rakopoulos, Giakoumis and Dimaratos, 2007). Also, $\tau_{\mathrm{fr}}(\varphi,\omega)$ stands for the friction torque during transient operation and is modelled as analysed in the previous sub-section. Finally, $\tau_{\mathrm{L}}(\omega)$ is the load torque, given by

$$\tau_{\mathrm{L}}=C_1+C_2\omega^{s}\,. \tag{21}$$

For a linear load-type (i.e. electric brake, generator) $s=1$, for a quadratic load-type (i.e. hydraulic brake, vehicle aerodynamic resistance) $s=2$, with C_1 the speed-independent load term (e.g. road slope).

3.3 Multi-cylinder engine modelling

At steady-state operation the performance of each cylinder of a multi-cylinder engine is practically the same, due to the (more or less) fixed position of the mechanical fuel pump rack position, resulting in the same amount of fuel being injected per cycle, and the fixed turbocharger compressor operating point resulting in the same air mass flow-rate for each cylinder.

On the other hand, under transient conditions each cylinder experiences different fuelling and air mass flow-rate during the same engine cycle. This is the result of the combined effect of

1 The continuous movement of the fuel pump rack, initiated by a load or speed change.

2 The continuous movement of the turbocharger compressor operating point.

As regards speed changes, only the first cycles are practically affected, but, when load changes are investigated (as is the case with the present study), significant variations can be experienced throughout the whole transient event.

The usual approach, here, is the solution of the governing equations for one cylinder and the subsequent use of suitable phasing images of this cylinder's behaviour for the others. This approach is widely applied due to its low computational time. Unlike this, a true multi-cylinder engine model is incorporated into the simulation code (Rakopoulos, Giakoumis and Hountalas, 1997; Rakopoulos and Giakoumis, 2006b). In this model, all the governing differential and algebraic equations are solved separately for each cylinder, according to the current values of fuel pump rack position and turbocharger compressor air mass flow-rate. This causes significant differences in the behaviour of each cylinder during the same transient cycle, affecting, among other things, engine response and exhaust emissions.

3.4 Fuel pump operation

Instead of applying the steady-state fuel pump curves during transients, a fuel injection model, experimentally validated at steady-state conditions, is used. Thus, simulation of the fuel pump-injector lift mechanism is accomplished, taking into account the delivery valve and injector needle motion (Rakopoulos and Hountalas, 1996). The unsteady gas flow equations are solved (for compressible injected fuel flow) using the method of characteristics, providing the dynamic injection timing as well as the duration and the rate of injection for each cylinder at each transient cycle. The obvious advantage here is that the transient operation of the fuel pump is also taken into account. This is mainly accomplished through the fuel pump residual pressure value, which is built up together with the other variables during the transient event.

4 Experimental procedure

The experimental investigation was carried out on a six-cylinder, four-stroke, moderately turbocharged and aftercooled diesel engine of 16.62 lit total displacement volume and rated power of 236 kW at 1,500 rpm.

The first task was the investigation of the steady-state performance of the engine in hand. For this purpose, an extended series of steady-state trials was conducted in order on the one hand to examine the model's predictive capabilities and, on the other, to calibrate successfully the individual sub-models described in Sections 2.2–3.4. The calibration procedure was based on matching simulated and experimental results concerning cylinder pressure diagram and exhaust emissions values. The calculated values of the constants of each sub-model, which are within the well established corresponding ranges (Benson and Whitehouse, 1979; Lipkea and DeJoode, 1994), remained then constant for all other examined cases. Typical results of the steady-state experimental study are given in Figures 1 and 2. An, overall, satisfactory agreement is observed between calculated and experimental data concerning cylinder pressure diagrams and exhaust emissions. Also, in the lower sub-diagram of Figure 1, the predicted temperatures of the two-zones are depicted together with the mean temperature (the latter calculated assuming isenthalpic mixing between the zones).

Figure 1 Calculated and experimental cylinder pressure diagrams, and calculated temperature of the unburned zone, the burned zone and the respective mean state at 75% load and 1,180 rpm

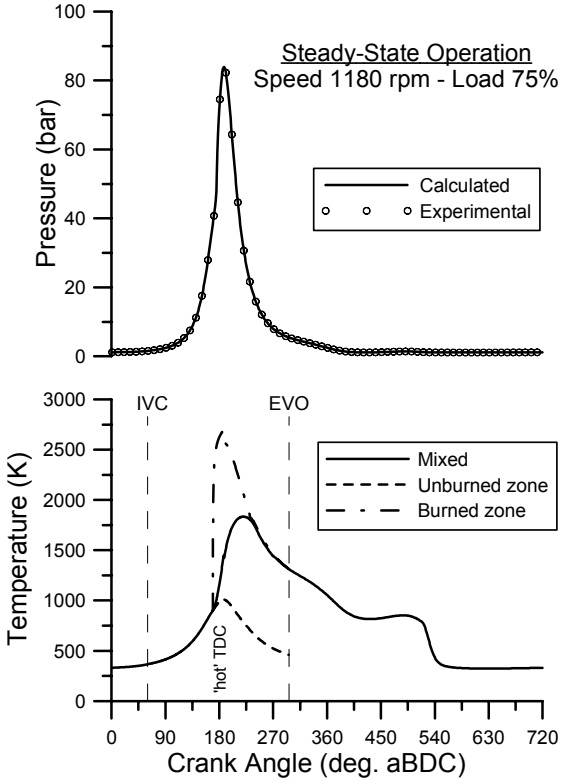

Figure 2 Nitric oxide concentration and soot density histories during steady-state operation and comparison with exhaust experimental values

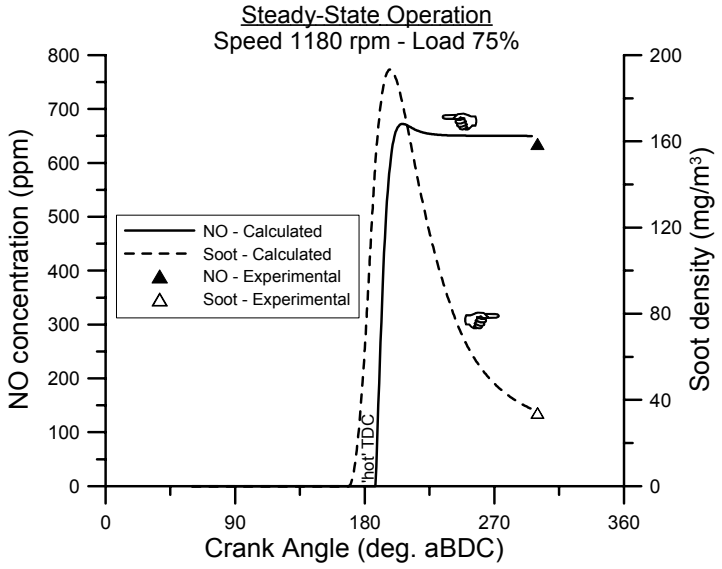

The next task was the investigation of the transient operation. Owing to the narrow speed range (1,000–1,500 rpm) of the particular engine, mainly load changes (increases) with constant governor setting were examined. An important feature of the engine under study is its very high mass moment of inertia (3–4 times greater than in similar configurations), which tends to limit the transient effects of the variables examined. Typical results of the experimental investigation are given in Figure 3 for 10–50% load increase commencing from 1,180 rpm. The non-linear character of the load application, which could not be accounted for in the simulation, is responsible for the small differences observed in boost pressure and engine speed response. The particular hydraulic brake has a very high mass moment of inertia, resulting in long, abrupt and non-linear actual load change profiles. Nonetheless, the matching between experimental and predicted transient responses seems satisfactory for all measured engine and turbocharger variables (engine speed, fuel pump rack position and boost pressure); it is thus believed to form a sound basis for the theoretical study of transient exhaust emissions that follows.

Figure 3 Experimental and predicted engine transient response to an increase in engine load

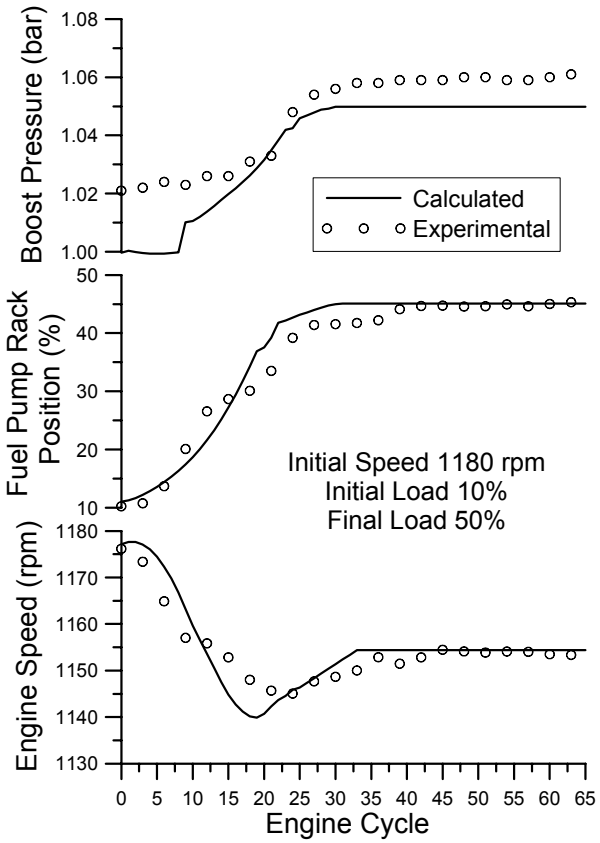

Figure 4 Development of various engine and turbocharger variables during a 10–80% load increase transient

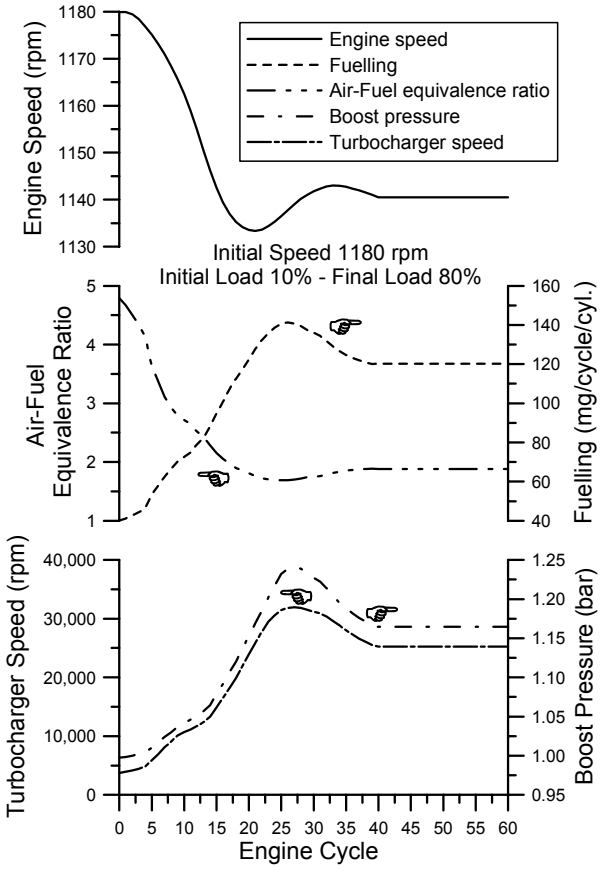

5 Results and discussion

Figure 4 illustrates the engine and turbocharger response during a 10–80% increase in engine load at constant governor setting, which forms the nominal case for the exhaust emissions analysis. As expected, engine speed drops after the application of the new higher load owing to torque deficit between engine and resistance. This is sensed by the governor, which responds by moving the fuel pump rack to an increased fuelling position. At the same time, turbocharger as well as the other system lags cause a delay in boost pressure build-up and, thus, shortage of combustion air resulting in rapid decrease of the air–fuel equivalence ratio (recall that aerodynamic type compressors cannot achieve high air mass flow-rates at low turbocharger speeds). However, the very high mass moment of inertia of the current engine slows down the whole transient event development and prevents complete combustion deterioration during the early cycles.

Figure 5 Development of nitric oxide concentration exhaust emission, maximum values of mean gas temperature and oxygen concentration in the fuel spray during a 10–80% load increase transient

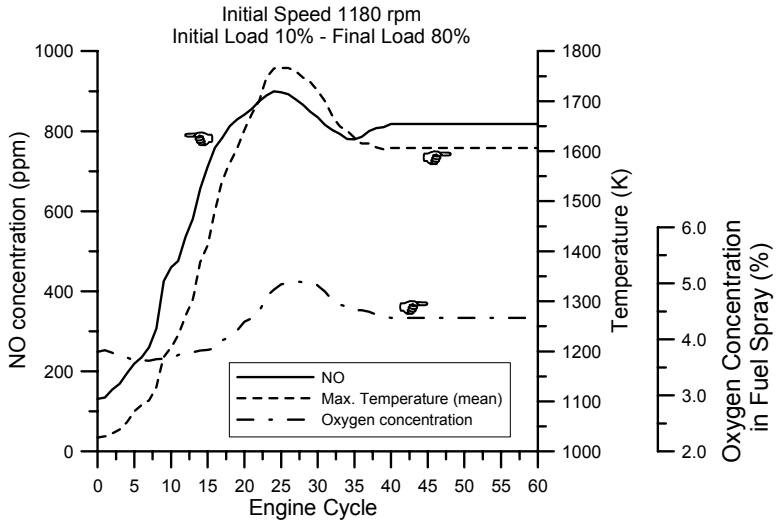

Figure 5 illustrates the development of the respective NO concentration exhaust emission during the load increase transient event; the maximum value of the mean (comprising both burned and unburned zones contribution) temperature in each transient cycle as well as the oxygen concentration in the fuel spray are also provided for comparison purposes. Initially, NO emissions are quite low owing to the low values of fuel-air equivalence ratio and charge temperature at the initial low loading. As the load increases, NO emissions increase too with its development following closely the temperature profile. This was intuitively expected based on the, well-known, strong dependence of NO formation on temperature (already documented in Equation (13) – see also next figure). In the case of NO emissions, it is primarily, the lag between increased fuelling and the response of the air-charging system that is responsible for the increased emissions noticed in Figure 5 (in engines equipped with EGR, the EGR starvation during the first cycles of a load increase or acceleration transient event enhances the above trend). On the other hand, the injection pressure and exhaust pressure history play a secondary, but non-negligible role (Hagena, Filipi and Assanis, 2006). Another important parameter is the duration of the load-change application, with 'instantly' applied loads leading to higher peaks of NO (and soot) emissions. Since the main parameter affecting NO formation is the burned gas temperature, local high temperatures due to close to stoichiometric air–fuel mixtures increase NO emissions during the turbocharger lag cycles as it is obvious in Figure 5 up to the 25th cycle. At the same time, the cylinder wall temperature is still low, as the 'thermal' transient develops much slower owing to the thermal inertia of the cylinder wall-coolant system (Benajes et al., 2002); this fact functions in an opposite manner, as it actually leads to higher heat transfer rates to the cylinder walls according to Equation (6), hence slight reduction of the gas temperature. The latter, however, only moderately limits the general strong and monotonic increasing trend of NO with Φ.

Figure 6 Development of nitric oxide concentration exhaust emission and its respective cumulative exhausted mass during transient operation for various cylinder wall insulation schemes

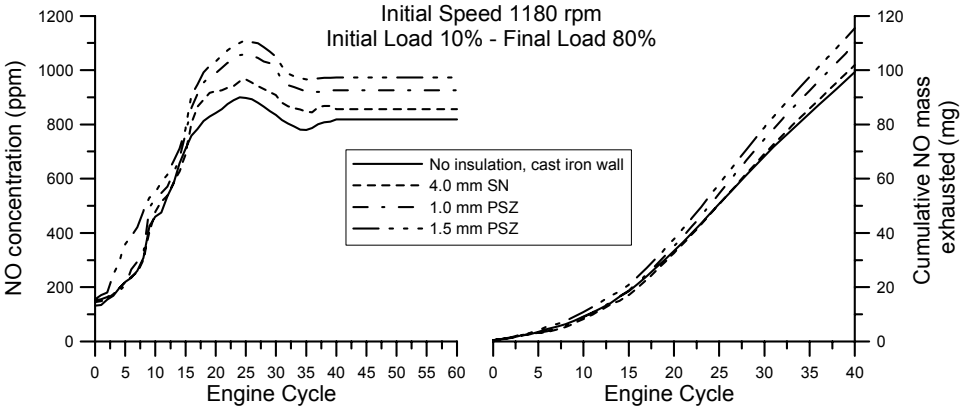

A second primary mechanism that affects NO formation is the in-cylinder oxygen availability. The latter parameter is illustrated in Figure 5 in terms of oxygen concentration in the fuel spray, where the conditions are mostly favourable for NO formation. Following the rapid decrease in the air–fuel ratio, oxygen concentration is rather limited during the turbocharger lag cycles. However, owing to the peculiarities of the particular engine (i.e. high mass moment of inertia that slows down the transient event) the relative air–fuel ratio never dropped below the stoichiometric value (see also Figure 4), which means that oxygen was always available for NO formation in the fuel spray.

The strong dependence of NO emissions on peak charge temperature during the transient event discussed previously can be further supported by the interesting case of cylinder wall insulation illustrated in Figure 6. Two common insulators are examined, namely plasma spray zirconia (PSZ; 1.0 and 1.5 mm coating) and silicon nitride (SN; 4.0 mm coating) for the same load increase transient event (Rakopoulos, Giakoumis and Rakopoulos, 2008). The objective of a low heat rejection cylinder is to minimise heat loss to the walls, eliminating the need for a cooling system. This is achieved at the expense of increased level of gas temperatures inside the cylinder resulting from the insulation applied to the cylinder walls, piston crown, cylinder head and/or valves. Following the increase in gas temperatures, the highly insulated wall cases exhibit higher NO emissions; the maximum difference observed in Figure 5 is 23.4% regarding (peak) concentration exhaust value and 16.2% regarding cumulative exhausted mass value for the 1.5 mm PSZ coating compared to the non-insulated engine operation.

Figure 7 focuses on the in-cycle development of NO concentration during two intermediate transient cycles compared to their respective steady-state counterparts, i.e. at the same engine speed and load (the latter being defined by brake mean effective pressure; BMEP). Unsurprisingly, differences between steady-state and transient NO emissions are observed concerning, mainly, their absolute values. On the other hand, the general development profile remains qualitatively unaltered for both operating modes.

NO concentration, as depicted in Figure 7, assumes higher in-cylinder maximum and higher 'exhaust' (i.e. at the point of exhaust valve opening) values during the transient cycles compared to its steady-state counterpart. This is, primarily, attributed to the higher cylinder gas temperatures during transients, resulting from higher values of fuel-air equivalence ratio; the latter being the direct consequence of turbocharger lag. Closer examination of the curves in Figure 7 reveals two other interesting facts. First, NO production practically lasts for a very small period, namely 20–25°CA. Second, NO during transients starts to evolve later in the cycle (a 'delay' of the order of 10°CA is observed compared to the respective steady-state cycles), implying that combustion begins later in the cycle, therefore the in-cylinder high temperatures occur later. This results from the combined effect of a variety of physical off-design phenomena occurring during transients, such as the later start of injection (originating from the lower values of fuel delivery system residual pressure), the increased ignition delay period and the overall slowing down of the whole combustion process (Rakopoulos and Giakoumis, 2006a).

Figure 7 Comparison of nitric oxide concentration histories for two intermediate transient cycles with their respective steady-state counterparts for a 10–80% load increase transient

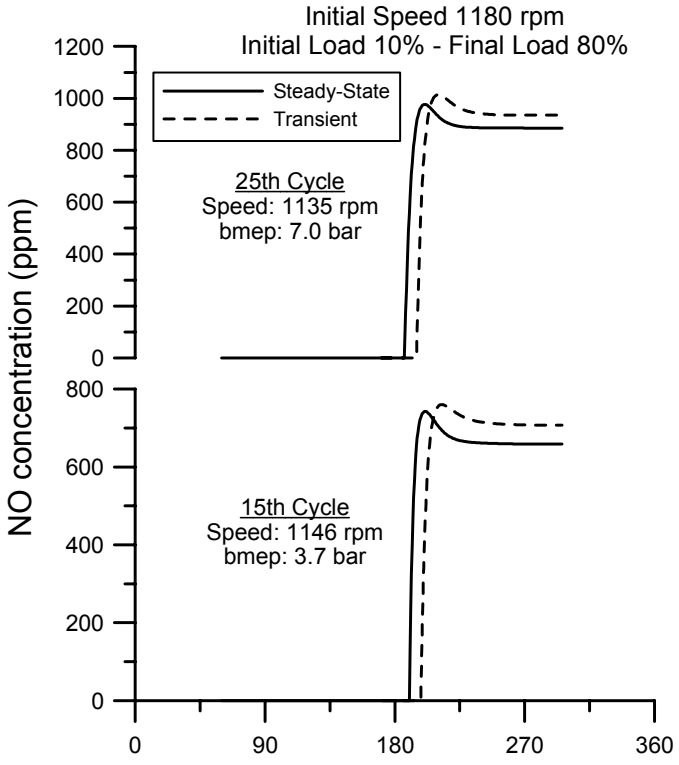

Figures 8–10 concentrate on the respective soot emission development during the same load increase transient.

Figure 8 Development of soot density exhaust emission, maximum values of mean gas temperature and fuel-air equivalence ratio during a 10–80% load increase transient

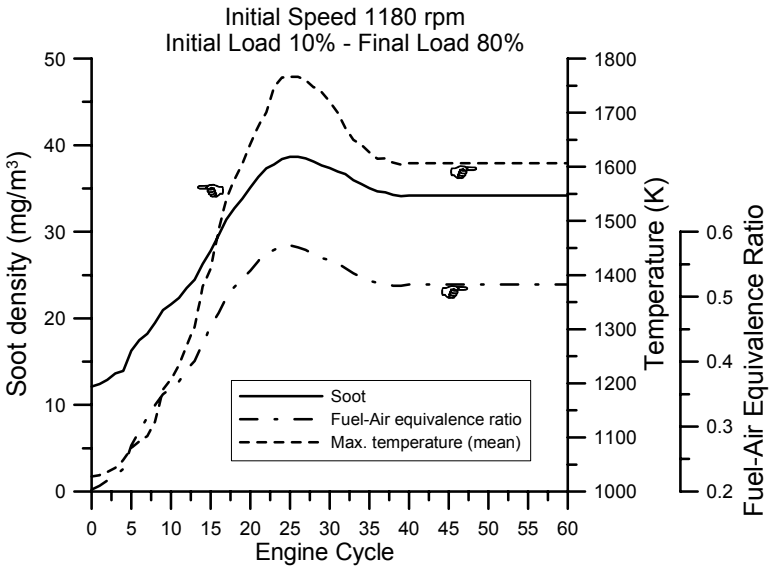

Figure 9 Development of soot density exhaust emission and its respective cumulative exhausted mass during transient operation for various load changes

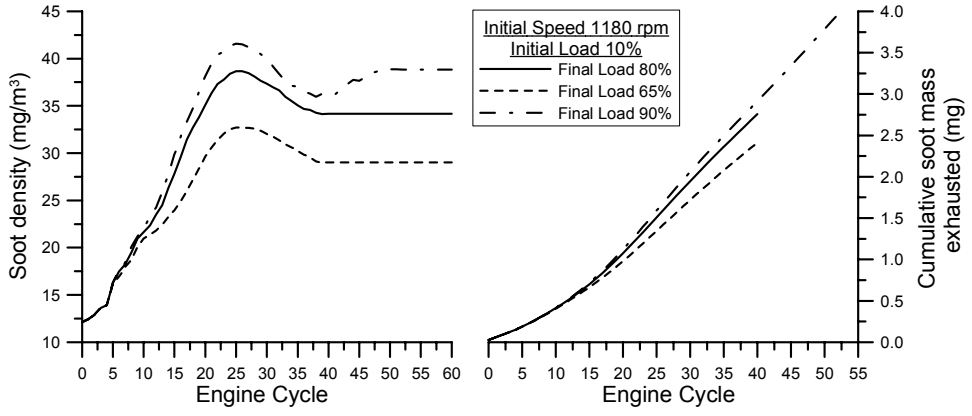

Figure 10 Comparison of soot density histories for two intermediate transient cycles with their respective steady-state counterparts for a 10–80% load increase transient

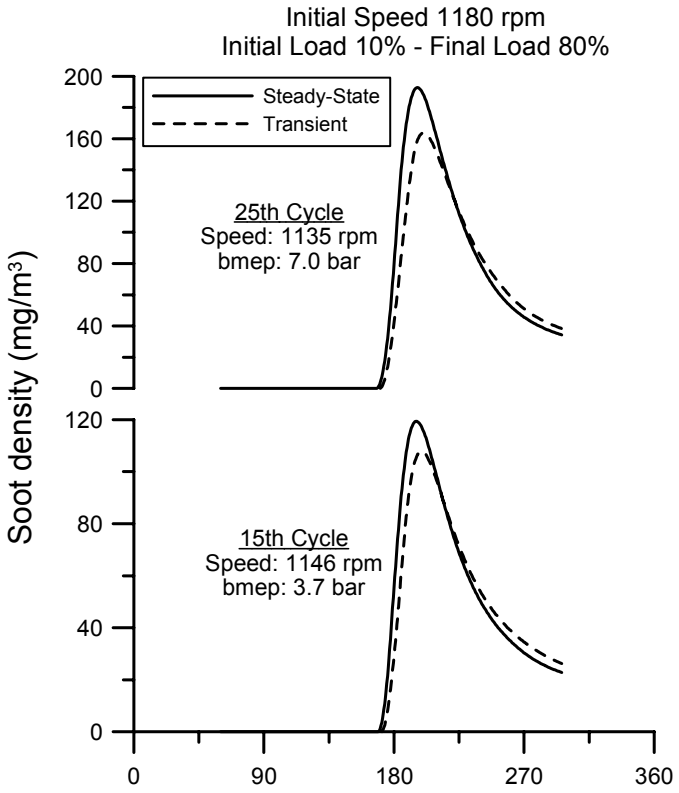

Figure 8 illustrates the soot density exhaust emission as well as the maximum value of the mean (comprising both burned and unburned zones contribution) temperature in each transient cycle and fuel-air equivalence ratio developments for the 10–80% load increase transient event. The formation of soot is mainly dependent on engine load (Heywood, 1988). As the load increases, more fuel is injected into the cylinders, increasing the temperatures in the fuel-rich zone during diffusion combustion; thus, the formation of soot is favoured. The local high values of fuel-air ratio experienced during turbocharger lag enhance the above mechanism, which is more pronounced the higher the engine rating. For the overshoot in soot emissions observed in the first seconds of the transient event of Figure 8, therefore, the main cause is the instantaneous lack of air due to turbocharger lag, aided by the initial sharp increase in ignition delay during the early transient cycles.

In order to further support the above remarks, Figure 9 highlights the effect of the magnitude of the applied load on transient soot formation. Both the soot density exhaust emission and its respective cumulative exhausted mass value (up to final steady-state cycle) are depicted in Figure 9. Obviously, the higher the applied load, the higher the (engine minus load) torque deficit during the early cycles of the transient event. This,

in turn, leads to a 'harder' turbocharger lag period, lower air–fuel ratio and engine speed, thus initiating larger governor displacement, greater fuel pump rack position, engine torque, cylinder peak pressure and turbocharger speed. Turbocharger lag effects are more pronounced the higher the applied load, a fact leading also to the higher (peak) soot density exhaust and cumulative exhausted mass values illustrated in Figure 9.

Figure 10 demonstrates in-cycle soot development during the 15th and 25th cycle of the transient event compared to the respective steady-state conditions. As for the case with NO (Figure 7), differences are noticed in the absolute values of soot density, while the development profile remains the same. The interesting finding from Figure 10 is that under transient conditions soot density assumes lower in-cylinder maximum, but higher exhaust values, compared to the respective steady-state conditions (same rotational speed and BMEP as the transient cycles). The latter indicates slower soot formation and oxidation. Indeed, soot formation and oxidation rates, as defined by Equations (16) and (17), respectively, are lower during turbocharger lag, owing to the previously discussed slowing down of the whole combustion process under such conditions, i.e. lower values of pressure, fuel mass burned at each time step and oxygen partial pressure in the fuel spray (the latter caused by poorer mixing). The result is that soot formation rate is actually lower during transients, but this holds also true for the respective oxidation rate during the expansion stroke; the latter is outweighed by its formation counterpart, ultimately leading to higher exhaust soot density values.

Finally, Figures 11 and 12 expand the previous remarks concerning NO and soot production during transients, providing a more detailed insight into these emissions formation mechanism. This is accomplished via 3D ('wave') illustration of the in-cycle emissions development for all cycles of the 10–80% load increase transient. In Figure 11, the late beginning of NO formation (discussed previously concerning Figure 7) is obvious at approximately 20°CA after 'hot' TDC for the first transient cycle, but gradually shifting earlier in the cycle as the transient event develops. Also, in Figure 12, the soot formation and oxidation processes during each transient cycle are clearly identified.

Figure 11 In-cycle nitric oxide concentration development for all cycles of a 10–80% load increase transient

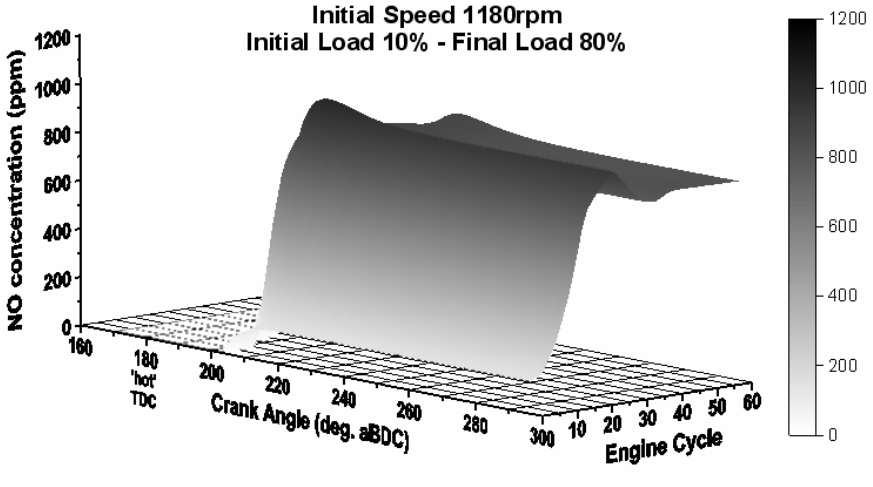

Figure 12 In-cycle soot density development for all cycles of a 10–80% load increase transient

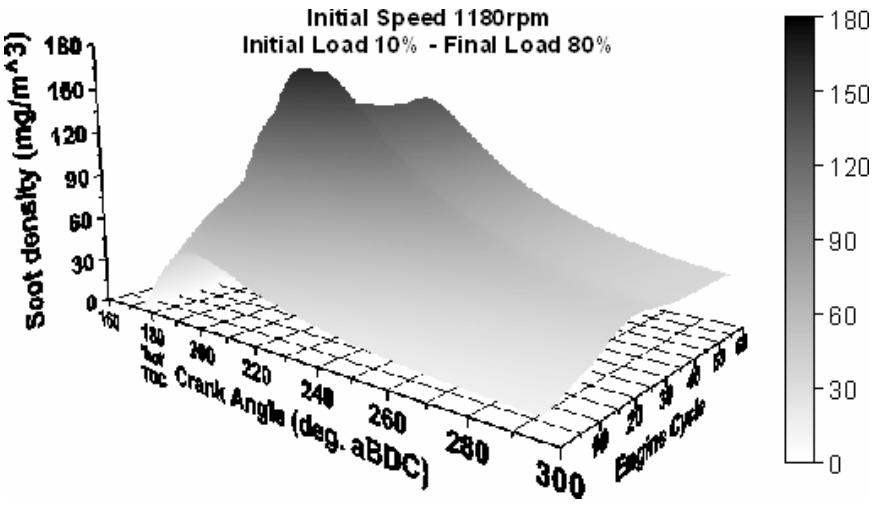

6 Conclusions

A comprehensive, two-zone, transient, diesel combustion model has been used for a preliminary estimation of NO and soot exhaust emissions during transient operation of a turbocharged diesel engine. Analytical modelling of in-cylinder processes has been developed, with detailed equations concerning all engine sub-systems, describing the peculiarities of transient operation. For the combustion chemistry, a complete chemical equilibrium scheme is used, except for the NO calculation, which is based on chemical kinetics consideration. A 10–80% load transient was investigated and individual intermediate transient cycles were compared with their steady-state counterparts (i.e. at the same engine speed and load) in terms of NO and soot formation. Moreover, the effect of the load change magnitude on soot emission and that of cylinder wall insulation on NO emission has been investigated. For the current engine-load configuration, the main findings of the study are summarised below:

- NO and soot emissions development during transient operation after a load increase follows closely the temperature and fuel-air equivalence ratio profiles, respectively, being strongly influenced by turbocharger lag.
- Transient exhaust emissions develop in a different way compared to the respective steady-state ones, owing to the differentiated fuelling and air-mass flow-rates experienced during transients. Both NO and soot emissions assume higher exhaust values during transients than in the respective steady-state conditions.
- NO formation is retarded for a few °CA during the transient cycles compared to steady-state conditions, owing to the overall slowing down of the whole combustion process during turbocharger lag.

- Soot formation and oxidation proceed more slowly during a transient cycle compared to its steady-state counterpart, resulting in lower in-cylinder maximum but higher exhaust values of soot density since the soot oxidation rate is actually lower than the formation one.
- The magnitude of the applied load directly affects exhaust emissions; increased values of soot emission are noticed for higher load changes, owing to the greater values of fuel-air equivalence ratio and charge temperature.
- Cylinder wall insulation affects strongly NO emissions through the significant increase in cylinder gas temperatures. The higher the degree of insulation, the higher the NO emissions observed.

A comprehensive experimental validation of the model's exhaust emissions results is under way.

References

Annand, W.J.D. and Ma, T.H. (1970–1971) 'Instantaneous heat transfer rates to the cylinder head surface of a small compression ignition engine', Proceedings of the *Institution of Mechanical Engineers*, Vol. 185, pp.976–987.

Arai, M., Tabata, M., Hiroyasu, H. and Shimizu, M. (1984) 'Disintegration process and spray characterisation of fuel jet injected by a diesel nozzle', *SAE Paper No. 840275*.

Bazari, Z. (1994) 'Diesel exhaust emissions prediction under transient operating conditions', *SAE Paper No. 940666*.

Benajes, J., Luján, J.M. and Serrano, J.R. (2000) 'Predictive modelling study of the transient load response in a heavy-duty turbocharged diesel engine', *SAE Paper No. 2000-01-0583*.

Benajes, J., Luján, J.M., Bermúdez, V. and Serrano, J.R. (2002) 'Modelling of turbocharged diesel engines in transient operation. Part 1: insight into the relevant physical phenomena', Proceedings of the *Institution of Mechanical Engineers, Part D: Journal of Automobile Engineering*, Vol. 216, pp.431–441.

Benson, R.S. and Whitehouse, N.D. (1979) *Internal Combustion Engines*. Oxford, UK: Pergamon Press.

Chan, S.H., He, Y. and Sun, J.H. (1999) 'Prediction of transient nitric oxide in diesel exhaust', Proceedings of the *Institution of Mechanical Engineers, Part D: Journal of Automobile Engineering*, Vol. 213, pp.327–339.

Hagena, J.R., Filipi, Z.S. and Assanis, D.N. (2006) 'Transient diesel emissions: analysis of engine operation during a tip-in', *SAE Paper No. 2006-01-1151*.

Heywood, J.B. (1988) *Internal Combustion Engine Fundamentals*. New York, NY: McGraw Hill.

Hiroyasu, H., Kadota, T. and Arai, M. (1983) 'Development and use of a spray combustion modelling to predict diesel engine efficiency and pollutant emissions', *Bulletin of the JSME*, Vol. 26, pp.569–583.

Kang, H. and Farell, P.V. (2005) 'Experimental investigation of transient emissions (HC and NO_x) in a high speed direct injection (HSDI) diesel engine', *SAE Paper No. 2005-01-3883*.

Lavoie, G.A., Heywood, J.B. and Keck, J.C. (1970) 'Experimental and theoretical study of nitric oxide formation in internal combustion engines', *Combustion Science and Technology*, Vol. 1, pp.313–326.

Lipkea, W.H. and DeJoode, A.D. (1994) 'Direct injection diesel engine soot modelling: formulation and results', *SAE Paper No. 940670*.

Rakopoulos, C.D. and Giakoumis, E.G. (2004) 'Availability analysis of a turbocharged diesel engine operating under transient load conditions', *Energy-The International Journal*, Vol. 29, pp.1085–1104.

Rakopoulos, C.D. and Giakoumis, E.G. (2006a) 'Review of thermodynamic diesel engine simulations under transient operating conditions', *SAE Paper No. 2006-01-0884*. Also, *SAE Transactions, Journal of Engines*, Vol. 115, pp.467–504.

Rakopoulos, C.D. and Giakoumis, E.G. (2006b) 'Sensitivity analysis of transient diesel engine simulation', Proceedings of the *Institution of Mechanical Engineers – Part D: Journal of Automobile Engineering*, Vol. 220, pp.89–101.

Rakopoulos, C.D. and Hountalas, D.T. (1996) 'A simulation analysis of a DI diesel engine fuel injection system fitted with a constant pressure valve', *Energy Conversion and Management*, Vol. 37, pp.135–150.

Rakopoulos, C.D., Giakoumis, E.G. and Dimaratos, A.M. (2007) 'Evaluation of various dynamic issues during transient operation of turbocharged diesel engine with special reference to friction development', *SAE Paper No. 2007-01-0136*.

Rakopoulos, C.D., Giakoumis, E.G. and Hountalas, D.T. (1997) 'A simulation analysis of the effect of governor technical characteristics and type on the transient performance of a naturally aspirated IDI diesel engine', *SAE Paper No. 970633*. Also, *SAE Transactions, Journal of Engines*, Vol. 106, pp.905–922.

Rakopoulos, C.D., Giakoumis, E.G. and Rakopoulos, D.C. (2008) 'Study of the short-term cylinder wall temperature oscillations during transient operation of a turbocharged diesel engine with various insulation schemes', *Int. J. Engine Research*, Vol. 9, pp.177–193.

Rakopoulos, C.D., Michos, C.N. and Giakoumis, E.G. (2005) 'Study of the transient behaviour of turbocharged diesel engines including compressor surging using a linearized quasi-steady analysis', *SAE Paper No. 2005-01-0225*.

Rakopoulos, C.D., Rakopoulos, D.C. and Kyritsis, D.C. (2003) 'Development and validation of a comprehensive two-zone model for combustion and emissions formation in a DI diesel engine', *Int. J. Energy Research*, Vol. 27, pp.1221–1249.

Rakopoulos, C.D., Giakoumis, E.G., Hountalas, D.T. and Rakopoulos, D.C. (2004a) 'The effect of various dynamic, thermodynamic and design parameters on the performance of a turbocharged diesel engine operating under transient load conditions', *SAE Paper No. 2004-01-0926*.

Rakopoulos, C.D., Rakopoulos, D.C., Giakoumis, E.G. and Kyritsis, D.C. (2004b) 'Validation and sensitivity analysis of a two-zone diesel engine model for combustion and emissions prediction', *Energy Conversion and Management*, Vol. 45, pp.1471–1495.

Shahed, S.M., Chiu, W.S. and Lyn, W.T. (1975) 'A mathematical model of diesel combustion', *Institution of Mechanical Engineers, Conference on 'Combustion in Engines*, Paper C94/75, pp.119–128.

Taraza, D., Henein, N. and Bryzik, W. (2000) 'Friction losses in multi-cylinder diesel engines', *SAE Paper No. 2000-01-0921*.

Watson, N. (1984) 'Eliminating rating effects on turbocharged diesel engine response', *SAE Paper No. 840134*.

Watson, N. and Janota, M.S. (1982) *Turbocharging the Internal Combustion Engine*. London, UK: McMillan.

Way, R.J.B. (1977) 'Methods for determination of composition and thermodynamic properties of combustion products for internal combustion engine calculations', Proceedings of the *Institution of Mechanical Engineers*, Vol. 190, pp.687–697.

Whitehouse, N.D. and Way, R.G.B. (1969–1970) 'Rate of heat release in diesel engines and its correlation with fuel injection data', Proceedings of the *Institution of Mechanical Engineers – Part 3J*, Vol. 184, pp.17–27.

Winterbone, D.E. (1986) 'Transient performance', in J.H. Horlock and D.E. Winterbone (Eds), *The Thermodynamics and Gas Dynamics of Internal Combustion Engines* (Vol. II, pp.1148–1212). Oxford, UK: Clarendon Press.

Appendix A

Fuel spray penetration and air entrainment rate

The correlation of Arai et al. (1984) is used for the spray tip location as a function of time, based on relevant experimental data and turbulent gas jet theory. The fuel injected inside the combustion chamber breaks up into globules, forming a cone-shaped spray corresponding to each one of the 'z' nozzle holes. If the kmoles of air trapped in the cylinder (in one cycle) are $w_{a_{tot}} = m_{a_{tot}} / M_a$, then the phenomenon will continue until each spray penetration reaches a value ($D/2 + \pi D/z$), or until it entrains a maximum quantity of air equal to $w_{a_{tot}}/z$.

Firstly, the parameters related to the fuel jet break-up point are calculated. The break-up time t_{br} is found by equating the two expressions of spray penetration correlation (Hiroyasu, Kadota and Arai, 1983) before and after t_{br}, corresponding to the break-up length $X = X_{br}$, which finally yield

$$t_{br} = \frac{28.61\rho_\ell \cdot D_N}{\sqrt{\rho_a \cdot \Delta p}},\ X_{br} = u_{inj} \cdot t_{br} \tag{A.1}$$

where Δp is the pressure drop across the injector nozzle, ρ_ℓ the liquid fuel density, ρ_a the density of air inside the cylinder and $u_{inj} = c_D\sqrt{2\Delta p / \rho_\ell}$ the spray velocity at the nozzle exit with c_D a discharge coefficient.

Accounting for air swirl, by introducing the air swirl ratio $R_s = N_s/N$ with N_s the cylinder charge rotational speed, the above correlations are modified as follows

$$X_{brs} = X_{br}\left(1 + \frac{\pi \cdot R_s \cdot N \cdot X_{br}}{30 \cdot u_{inj}}\right)^{-1},\ t_{brs} = \left(\frac{X_{brs}}{X_{br}}\right) t_{br} \tag{A.2}$$

After the calculation of the fuel jet break-up point characteristics, the following cases are discriminated, according to the value of time t.

For $t \le t_{brs}$

$$X = u_{inj} \cdot t,\ X_s = X\left(1 + \frac{\pi R_S N \cdot X}{30 u_{inj}}\right)^{-1},\ \theta = 0,\ \theta_s = 0 \tag{A.3}$$

For $t > t_{brs}$

$$\begin{aligned} &X = 2.95\left(\frac{\Delta p}{\rho_a}\right)^{0.25} \sqrt{D_N} \cdot t^\beta,\ X_s = X\left(1 + \frac{\pi R_s N \cdot X}{30 u_{inj}}\right)^{-1} \\ &\theta = 2\arctan\left(\frac{1}{A'} 4\pi \sqrt{\frac{\rho_a}{\rho_\ell}} \frac{\sqrt{3}}{6}\right),\ \theta_s = \theta \cdot \left(\frac{X}{X_s}\right)^2 \end{aligned} \tag{A.4}$$

where $A' = 3 + 0.28(L_N / D_N)$ (Heywood, 1988).

The mass of entrained air in the spray (of conical shape) is

$$m_{\mathrm{a}} = \frac{\pi}{3}\left(\tan\frac{\theta}{2}\right)^2 \cdot \rho_{\mathrm{a}} \cdot (X - X_{\mathrm{br}})^3$$
$$m_{\mathrm{a_s}} = \frac{\pi}{3}\left(\tan\frac{\theta_{\mathrm{s}}}{2}\right)^2 \cdot \rho_{\mathrm{a}} \cdot (X_{\mathrm{s}} - X_{\mathrm{brs}})^3 \tag{A.5}$$

where in the above relations it is considered that the volume taken by the fuel is negligible against that of the air, as well as the paraboloid part at the base of the cone against that of the pure cone.

The above relations for the air mass entrained into the fuel spray apply only in the case where $t_{\mathrm{brs}} < t \le (\Delta\varphi_{\mathrm{inj}} / 6N) + t_{\mathrm{brs}}$. In the case where $t > (\Delta\varphi_{\mathrm{inj}} / 6N) + t_{\mathrm{brs}}$, a conical part at the tail (index t) of the spray has to be subtracted. Then, the above equations become

$$m_{\mathrm{a}} = \frac{\pi}{3}\rho_{\mathrm{a}}\left(\tan\frac{\theta}{2}\right)^2 (X - X_{\mathrm{br}})^3 - \frac{\pi}{3}\rho_{\mathrm{a}}\left(\tan\frac{\theta_{\mathrm{t}}}{2}\right)^2 (X_{\mathrm{t}} - X_{\mathrm{br}})^3$$
$$m_{\mathrm{a_s}} = \frac{\pi}{3}\rho_{\mathrm{a}}\left(\tan\frac{\theta_{\mathrm{s}}}{2}\right)^2 (X_{\mathrm{s}} - X_{\mathrm{brs}})^3 - \frac{\pi}{3}\rho_{\mathrm{a}}\left(\tan\frac{\theta_{\mathrm{ts}}}{2}\right)^2 (X_{\mathrm{ts}} - X_{\mathrm{brs}})^3 \tag{A.6}$$

where $X_{\mathrm{t}} = 2.95(\Delta p / \rho_{\mathrm{a}})^{0.25}\sqrt{D_{\mathrm{N}}}[t - (\Delta\varphi_{\mathrm{inj}} / 6N) - t_{\mathrm{br}}]^{\beta_{\mathrm{t}}}$ is the cone length to be subtracted in the case of no-swirl and $X_{\mathrm{ts}} = X_{\mathrm{t}}(1 + \pi R_{\mathrm{s}} N \cdot x / 30u_{\mathrm{inj}})^{-1}$ is the corresponding cone length to be subtracted when swirl exists.

Finally, the corresponding spray angles for the tail part of the cone to be subtracted are, respectively

$$\theta_{\mathrm{t}} = \theta, \theta_{\mathrm{ts}} = \theta_{\mathrm{t}}\left(\frac{X_{\mathrm{t}}}{X_{\mathrm{ts}}}\right)^2. \tag{A.7}$$